Journal of
NANOSTRUCTURES
JNS
NANOSTRUCTURES
JNS.kashanu.ac.ir

The Effect of Annealing, Synthesis Temperature and Structure on Photoluminescence Properties of Eu-Doped ZnO Nanorods

M. Najafi*, H. Haratizadeh, M. Ghezellou

Department of Physics, Shahrood University, University Blvd, 3619995161 Shahrood, Iran.

Article history:
Received 08/04/2015
Accepted 12/05/2015
Published online 01/06/2015

Keywords:
ZnO
CVD
Photoluminescence
Nanorod

**Corresponding author:*
E-mail address:
najafi@shahroodut.ac.ir
Phone: + 98 2332392205
Fax: + 98 2332392206

Abstract

In this study un-doped and Eu-doped ZnO nanorods and microrads were fabricated by Chemical Vapor Deposition (CVD) method. The effects of annealing, synthesis temperature and structure on structural and photoluminescence properties of Eu-doped ZnO samples were studied in detail. Prepared samples were characterized using X-Ray diffraction (XRD), scanning electron microscopy (SEM), particle size analysis (PSA) and Photoluminescence Spectroscopy (PL) analysis. XRD results indicated that all of samples have a wurtzite structure and Eu^{3+} ions were incorporated successfully into the lattice of ZnO nanostructures. SEM and PSA analysis exhibit nanorads rather than microrads samples have a more surface to volume ratio which cause to enhance surface defects. This study recommends that energy transfer (ET) from ZnO host to Eu ions via intrinsic defects at indirect excitation. By annealing due to decease of intrinsic defects particularly oxygen vacancy ET and consequently Eu ions emissions are decreased considerably. Pl analysis exhibit relative intensities of the electric-dipole and magnetic-dipole transitions were changed in different growth conditions.

1. Introduction

Metal oxide semiconductor films have been widely used for various applications due to their excellent optical and electrical properties. Among metal oxides, zinc oxide (ZnO) nanostructures have been of great interest due to their potential applications in many significant fields such as solarcells, light emitting diodes (LED) and optoelectronic devices [1-6]. ZnO is a II-VI semiconductor with a large direct band gap of 3.37

eV and a relatively large exciton binding energy of 60 meV with many interesting optical properties [7-9]. Understanding the role of defects and the carrier recombination processes in ZnO nanostructures is an essential part of optoelectronic devices development. ZnO is characterized by two main emission bands in its PL spectrum. The UV emission band is related to a near band-edge (NBE) transition of ZnO and deep level emission band (DLE). The DLE band has previously been attributed to several defects in the crystal structure such as O-vacancy (V_O) [10-17], O-interstitial (O_i) [18, 19], Zn-vacancy (V_{Zn}) [20, 21], Zn-interstitial (Zn_i) [15], O-antisite (O_{Zn}) [21] and extrinsic impurities such as substitutional Cu [22]. In addition, regarding to variety of defect levels in the wide band gap energy of ZnO, this semiconductor is a suitable host for rare-earth (RE) ions, which are optically and magnetically active [23]. Since direct excitation of the parity forbidden 4f–4f transitions of Ln^{3+} is generally inefficient in comparison with the host absorption in UV region[24], Ln^{3+} ions embedded in wide band-gap semiconductors. Among RE ions, Eu^{3+}ions have been extensively studied due to their red-light emission [10]. In this work, effects of annealing, synthesis temperature and structure on structural and photoluminescence properties of Eu-doped ZnO nanostructures are examined. The effective role of intrinsic defects on energy transfer to Eu ions investigated in detailed. Since lanthanides luminescence long life time are in the range of microseconds to milliseconds, for better investigation of defects effect on red emission, phosphorescence spectroscopy employed besides of fluorescence spectroscopy, which its decay time is in the same region of lanthanides luminescence lifetime.

2. Experimental procedure

All chemicals were purchased from Merck and Aldrich companies with analytic grade reagents and without any further purification. The samples were deposited on silicon wafer substrates which were cleaned by sonication in acetone bath. Un-doped and Eu-doped ZnO Nanorods and microrads were grown through chemical vapor deposition (CVD) on Si substrate. A mixture of Zn and 1 mol % EuCl3.6H2O powders was placed at the middle of high-temperature zone in a furnace. One of the substrates was placed directly above the initial material and the other was placed at a distance of 10 cm from the source. The furnace was heated to 650°C under flowing Ar with a flow rate of 80 standard cubic centimeters per minute (SCCM). When the temperature reached the synthesis temperature, high purity oxygen gas with 6N purity was introduced into the quartz tube with a flow rate of 10 SCCM for growth of ZnO nanorods. The growth time of the process was 1 hr before terminating the oxygen flow and cooling down to room temperature. In addition, other un-doped and Eu-doped samples according to table 1 were prepared with the same procedure to investigate the effect of growth temperature, structure, annealing in air at 400°c and the ratio of Ar/O_2 on photoluminescence properties.

Table 1. different growth conditions of ZnO samples

Sample Number	Material and Doping	Structure	Annealing	Ar/O_2 ratio	Growth Temperature
Sample 1	Un-doped ZnO	Nanorads	As-Grown	8	650°c
Sample 2	Un-doped ZnO	Microrads	As-Grown	8	650°c
Sample 3	Un-doped ZnO	Nanorads	Annealed	8	650°c
Sample 4	Eu-doped ZnO	Nanorads	As-Grown	8	750°c
Sample 5	Eu-doped ZnO	Nanorads	As-Grown	8	650°c
Sample 6	Eu-doped ZnO	Nanorads	As-Grown	4	650°c
Sample 7	Eu-doped ZnO	Microrads	As-Grown	8	650°c
Sample 8	Eu-doped ZnO	Nanorads	Annealed	8	650°c
Sample 9	Eu-doped ZnO	Microrads	Annealed	8	650°c

The crystal structure quality and the phase identification of products obtained were characterized by X–ray diffractometer (XRD) with Ni–filtered Cu–Kα radiation. Moreover morphology of the samples was examined by field emission scanning electron microscope (FESEM, JEOL JSM–6700F). Room temperature photoluminescence spectra were taken on a Perkin–Elmer LS55 spectrophotometer equipped with a 450W Xe lamp as excitation source. Particle size distribution of ZnO samples were investigated using Particle Size analyzer (Mastersizer 2000 Ver. 5.1).

3. Results and discussion

Fig.1 shows comparative XRD patterns of sample 1, sample 2 and sample 3. All peaks in the X-ray diffraction pattern are assigned to the typical wurtzite structure of ZnO. There are no other diffraction peaks originating from europium or any other impurities in the XRD data. It indicates the Eu^{3+} ions have been incorporated successfully into the ZnO lattice without any amorphous component and other additional crystalline phase. The inset on the right shows the shift of main peak positions in detail. The positions of the main diffraction peaks shifted to low diffraction angle by doping of Eu^{3+} ions in ZnO lattice. This shift indicates the effective substitution of Eu^{3+} ions instead of Zn^{2+} ions into the ZnO crystal lattice. This phenomenon could be explained by the different radius of Eu^{3+} with Zn^{2+} ions. The ionic radius of Eu^{3+}ion (95 pm) is larger than Zn^{2+}ion (74 pm). By Eu doping (sample 5), the intensity of peaks decreases (rather than sample1) indicating that Eu dopind deteriorates crystallinity of the sample. However, it is observed that after annealing (sample 3), the crystallinity of the ZnO nanorods was improved, and consequently the intensity of the diffraction peaks was enhanced considerably in comparison with the as-grown ZnO nanorods (sample 1).

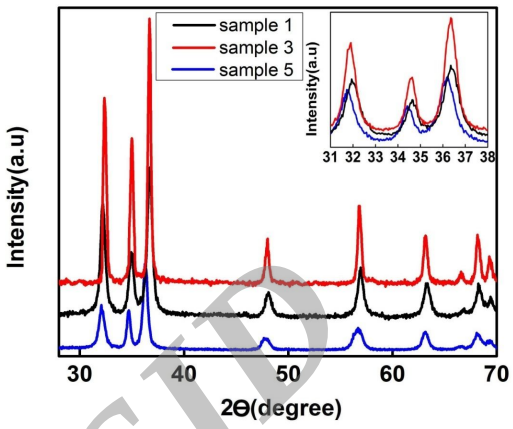

Fig. 1. Comparative XRD patterns of sample 1, sample 2 and sample 3.

Fig.2a and Fig.2b show SEM images of ZnO:Eu nanorods (sample5) and microrads (sample7), respectively. It indicates that diameter of nanorods is between 10 to 20 nm and length of nanorods is around 1μm. Also Fig.2b exhibits that diameter of microrads is between 0.5 to 2 μm and length of microrads is around 5μm.

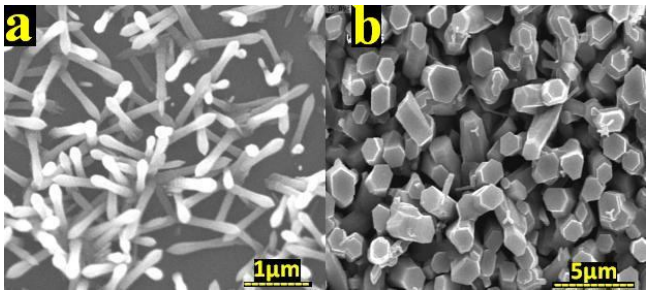

Fig. 2. (a) SEM images of ZnO:Eu nanorods (sample5) and (b) microrads (sample7).

The particle size distribution of Eu–doped ZnO nanorods (sample5) and microrods (sample7) samples are shown in Fig.3 and Fig.4, respectively. It indicates that size of ZnO:Eu nanorod particles is smaller than ZnO:Eu microrods. Particle size

analyzer measures the average size of separated particles. In ZnO:Eu nanorods sample, the measured particle size is attributed to length of nanorads rather than their diameter. It indicates that average size of nanorods is mostly around 1μm and In the case of ZnO:Eu microrods sample, the result shows the average size of microrods is mostly around 4μm.

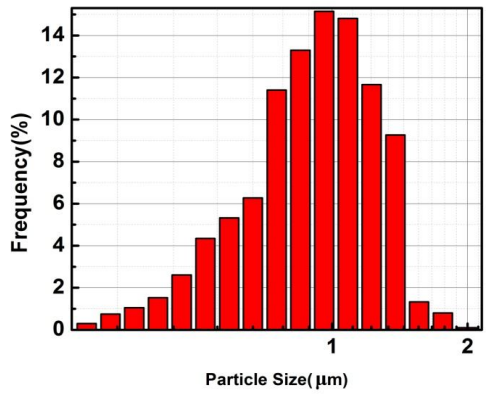

Fig.3. Particle size distribution of Eu–doped ZnO microrods (sample7).

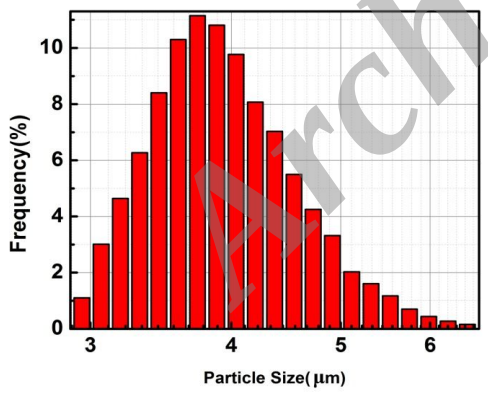

Fig.4. Particle size distribution of Eu–doped ZnO nanorods (sample5).

Fig.5 shows the photoluminescence excitation (PLE) spectrum of Eu-doped ZnO nanorods (sample5) monitored at 615nm. It illustrates direct excitation peaks at 464nm and 425nm attributed to $^7F_0$–$^5D_2$ and $^7F_0$–$^5D_3$ transitions of Eu^{3+} ions, respectively and also other indirect excitation peaks particularly strong excitation peak at 390nm corresponded to the NBE in the Eu-doped ZnO.

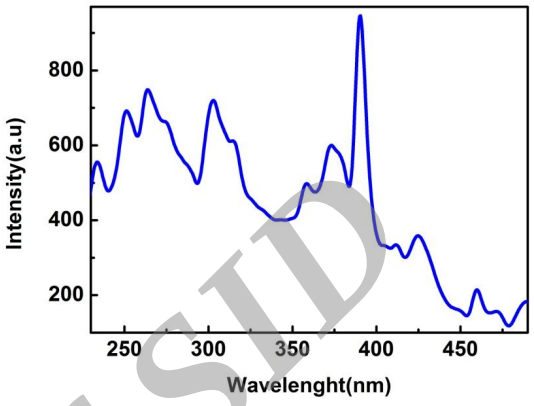

Fig.5. Photoluminescence excitation (PLE) spectrum of Eu-doped ZnO nanorods (sample5) monitored at 615nm

Fig.6 shows the room temperature fluorescence spectra of as-grown (sample 1) and annealed (sample3) ZnO nanorods samples and also microrads (sample 2) sample under the excitation at 325 nm. It indicates that UV emission band centered at 390 nm is attributed to NBE emission of ZnO samples. However, the broad defect emission is related to blue and green emissions centered at about 430, 500 and 530nm. These emissions are resulted from the recombination of photo-generated hole with a singly ionized charge state of specific defect which is consistent with intrinsic defects such as Zn_i, V_{Zn} and V_O. The green emission is attributed to V_O and the blue emission is assigned to the electron transition from both of the conduction band to the V_{Zn} levels and the Zn_i level to top of the valence band. The energy of blue emission (430nm) is close to the photon energy excited of Eu^{3+} ions at 425nm attributed to $^7F_0$–$^5D_2$ transition and the energies of green emissions (500 and 530nm) are close to the photon energy excited

of Eu^{3+} ions at 464nm and 510nm attributed to $^7F_0$–$^5D_2$ and $^7F_3$–$^5D_2$ transitions, respectively. After annealing in the air, the intensity of the defect-related blue and green emissions and also the Eu^{3+} related red emissions are quenched considerably. By annealing in the air the green emission attributed to oxygen vacancy was decreased. In nanorods spectrum in comparison with microrads sample, strong green emission was observed. ZnO nanorods have a high surface area-to-volume ratio, which results in a high level of surface defects such as oxygen vacancies. It is obvious that the red emission intensity was enhanced with increasing of deep level emission, particularly blue and green ones, which are attributed to zinc and oxygen vacancies respectively. Since the energies of these defects are well matched with the energies of intra 4f transitions of Eu^{3+}, it is clear that the Eu^{3+} ions absorb the energy via defects of ZnO nanostructures.

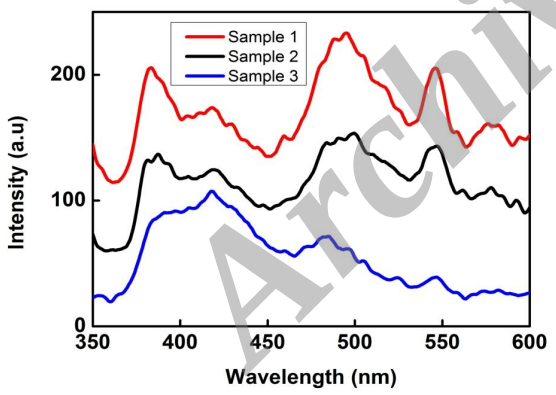

Fig.5. Fluorescence spectra of as-grown (sample1) and annealed (sample 3) ZnO nanorods samples and also microrads (sample 2) sample under the excitation at 325 nm.

Fig.7 illustrates the room temperature phosphorescence spectra of as-grown and annealed Eu-doped ZnO samples in different growth conditions corresponding with table 1 under the excitation at 390nm. There are two sharp emission peaks at 589 and 613nm. These emissions are attributed to the $^5D_0 \rightarrow {}^7F_J$ (J=1–2) transitions of the Eu^{3+} ions, respectively. The energies of all these peaks are well matched with the energies of intra4f transitions of Eu^{3+} ions [25]. $^5D_0 \rightarrow {}^7F_2$ emission arising from an electric-dipole transition, which results in a large transition probability in the crystal fields with inversion antisymmetry [26]. It is believed that Eu^{3+} ions occupy a site with inversion symmetry since $^5D_0 \rightarrow {}^7F_1$ transition originates from a magnetic-dipole transition. A lower symmetry around Eu^{3+} ion would result in a higher I ($^5D_0$-$^7F_2$)/I($^5D_0$-$^7F_1$) value, known as a asymmetric factor or asymmetric ratio[26]. The inset on the left of Fig7 shows the relative intensities of the electric-dipole and magnetic-dipole transitions. It exhibits that the relative intensities which shows local symmetry of Eu^{3+} ions, strongly depends on growth conditions. It is shown in comparison with sample 5, by increasing synthesis temperature to 750°C (sample 4) the intensity of red emission was enhanced, which confirms our hypothesis that expresses in higher temperatures more Eu^{3+} ions are incorporated in ZnO lattice. It is obvious when the ratio of Ar/O_2 reduced to 4 (sample 6), consequently the relative intensities of the electric-dipole and magnetic-dipole transitions decreased which attributed to decrease in Oxygen vacancy defects. In comparison with Eu-doped ZnO nanorods (sample 5), Eu-doped ZnO microrods (sample 7) have a less surface area and consequently possess a few surface defects. Moreover, it is shown that after annealing the intensity of red emission in Eu-doped ZnO nanorods (sample 8) and Eu-dopd ZnO microrods (sample 9) decreased, which was correlated to corresponding decrease in oxygen deficiency.

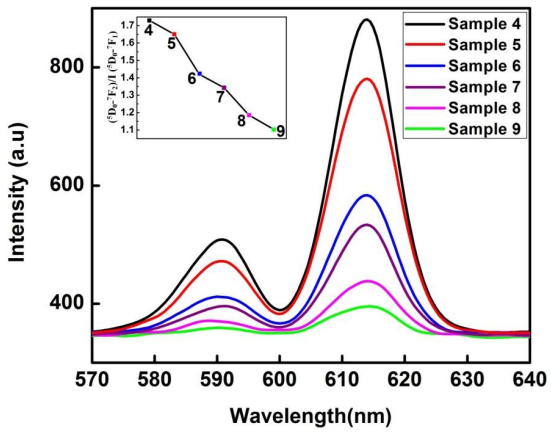

Fig. 7. Phosphorescence spectra of as-grown and annealed Eu-doped ZnO samples in different growth conditions corresponding with table 1 under the excitation at 390nm.

4. Conclusion

In summary, un-doped and Eu-doped ZnO samples were synthesized through the CVD method. Effects of annealing, synthesis temperature, atmosphere ratio and structure on structural and photoluminescence properties of the ZnO nanorods and microrads samples were investigated in detail, using XRD, SEM, PSA and PL analysis. According to the XRD analysis, Eu^{3+} ions were incorporated successfully into the lattice of ZnO nanostructures. The PL spectra analysis demonstrated a correlation between defect states and energy transfer from the ZnO to the Eu^{3+} ions, which consequently led to strong red emission. Pl results also revealed relative intensities of the electric-dipole and magnetic-dipole transitions were modified in different growth conditions. After annealing, both defects and Eu^{3+} related red emissions were considerably quenched. Decrease in the red emissions was correlated with corresponding decrease in oxygen deficiency. Moreover, in nanoscale samples comparing to microscale samples due to more surface defects there was more energy transfer to Eu ions. The results indicated to effective role of intrinsic defects on energy transfer from ZnO host to Eu^{3+} ions and consequently led to producing the strong red emission from these sites.

References

[1]. Ü. Özgür, Y. I. Alivov, C. Liu, A. Teke, M. A. Reshchikov, S. Dogan, V. Avrutin, S. J. Cho, H. Morkoc, J. Appl. Phys. 98 (2005) 041301.

[2]. N. H. Alvi, K. ul. Hasan, O. Nur, M. Willander, Nanoscale Res. Lett. 6 (2011) 130.

[3]. S. Chakraborty, A. K. Kole, P. Kumbhakar, Mat Lett. 67 (2012) 362–364.

[4]. L. L. Yang, Q. X. Zhao, M. Willander, J. H. Yang, I. Ivanov, J. Appl. Phys. 105 (2009) 053503.

[5]. J. Ji, L. A. Boatner, F. A. Selim, Appl. Phys. Lett. 105 (2014) 041102.

[6]. F. A. Selim, M. H. Weber, D. Solodovnikov, K. G. Lynn, Phys. Rev. Lett. 99 (2007) 085502.

[7]. J. L. Gomez, O. Tigli, J Mater Sci. 48 (2013) 612–624.

[8]. E. Koushki, M. H. Majlesara, S.H. Mousavi, H. Haratizadeh, Curr. Appl. Phys. 11 (2011) 1164-1167

[9]. M. Willander, Y. E. Lozovik, Q.X. Zhao, O. Nur, Q.H.Hu, and P. Klason, Proc. SPIE Vol. 6486 (2007) 648614.

[10]. Z. N. Urgessa, O. S. Oluwafemi, J. K. Dangbegnon, J.R.Botha, Physica B. 407 (2012) 1546–1549.

[11]. N. Y. Garces, L. Wang, L. Bai, N. C. Giles, L. E. Halliburton, G. Cantwell, Appl. Phys. Lett. 81 (2002) 622.

[12]. X. O. Meng, D. Z. Shen, J. Y. Zhang, D. X. Zhao, Y. M. Lu, L. Dong, Z. Z. Zhang, Y. C. Liu, X. W. Fan, Sol. Stat. Comm. 135 (2005) 179.

[13]. N. E. Hsu, W. K. Hung, Y. F, Chen J. Appl. Phys. 96 (2004) 4671.

[14]. A. V. Dijken, E. A. Meulenkamp, D. Vanmaekelbergh, and A. Meijerink, J. Lumm. 90 (2000) 123.
[15]. K. Vanheusden, C. H. Seager, W. L. Warren, D. R. Tallant, J. A. Voigt, Appl. Phys. Lett. 68 (1996) 403.
[16]. F. Leiter, H. Alves, D. Pfisterer, N. G. Romanov, D. M. Hofmann, B. K. Meyer, Phys. B (2003) 201.
[17]. S. H. Jeong, B. S. Kim, B. T. Lee, Appl. Phys. Lett. 82 (2003) 2625.
[18]. H. S. Kang, J. S. Kang, S. S. Pang, E. S. Shim, S. Y. Lee, Mater. Sci. Eng. B 102 (2003) 313.
[19]. X. Liu, X. Wu, H. Gao, R. P. H. Chang, J. Appl. Phys. 95 (2004) 3141.
[20]. M. Liu, A. H. Kitai, P. Mascher, J. Lumm. 54 (1992) 35.
[21]. Y. W. Heo, D. P. Norton, S. J. Pearton, J. Appl. Phys. 98 (2005) 073502.
[22]. Q. X. Zhao, P. Klason, M. Willander, H. M. Zhong, W. Lu, J. H. Yang, Appl. Phys. Lett. 87 (2005) 211912.
[23]. P. Chea, J. Mengb, L. Guoa, J. Lumm. 122–123 (2007) 168–171
[24]. Y. Sh. Liu, W. Luo, H. Zhu, X. Chen, J. Lumm. 131 (2011) 415–422.
[25]. Y. P. Du, Y.W. Zhang, L.D. Sun, C.H. Yan, J. Phys. Chem. C 112 (2008) 12234.
[26]. P. Dorenbos, L. Pierron, L. Dinca, C. V. Eijk, A. K. Harari, B. Viana, J. Phys. Condens. Matter 15 (2003) 511. [17] G.N. Glavee, K.J. Klabunde, C.M. Sorensen. G.C. Hadjapanyis, Languir. 8 (1992) 771–773.